Heliyon 10 (2024) e34098

Contents lists available at ScienceDirect

Heliyon

journal homepage: www.cell.com/heliyon

Research article

A clinically-recommended MR whole lung imaging protocol using free-breathing 3D isotropic zero echo time sequence

Qiuxi Lin [a,1], Cheng Cheng [a,b,1], Yingying Bao [a], Weiyin Vivian Liu [c], Lei Zhang [c], Zhaofeng Cai [a], Qi Wan [a], Chongpeng Sun [a], Xinchun Li [a], Yu Deng [a,*]

[a] Department of Radiology, The First Affiliated Hospital of Guangzhou Medical University, Guangzhou, 510120, China
[b] Department of Radiology, LIWAN Central Hospital of GUANGZHOU, 510120, China
[c] MR Research, GE Healthcare, Beijing, 100176, China

ARTICLE INFO

Keywords:
Magnetic resonance imaging
Zero echo time imaging
Zero TE
Lung
Short T2 imaging

ABSTRACT

Rationale and objectives: This study aimed to assess the feasibility and image quality of free-breathing 3D isotropic zero echo time (ZTE) whole-lung imaging and explore a clinically appropriate protocol for MR lung imaging.

Materials and methods: The study was approved by the local ethics committee. A total of thirty healthy volunteers were enrolled in this study from October 2022 to May 2023. Free-breathing pulmonary 3D isotropic ZTE scans were implemented with various acquisition planes and the number of excitations (NEX). ZTE images were evaluated by two radiologists for the overall Image quality and visibility of intrapulmonary structures as well as the signal-to-noise ratio (SNR) of the lung parenchyma. ZTE images with different acquisition parameters were compared. For preliminary clinical visual assessment, three patients with interstitial lung disease underwent both ZTE imaging and computed tomography (CT).

Results: The overall image quality of the lung in healthy subjects was good to excellent. The visibilities of pulmonary arteries and bronchus were up to the 7th and 5th generation, respectively. The display of lung fissures was poor. The overall image quality, the visibility of the pulmonary artery, and lung fissures in the axial acquisition were better than in the coronal acquisition ($P = 0.011$, 0.008, 0.010, respectively) but not statistically different from those in the sagittal acquisition (all $P > 0.05$).

Conclusion: The free-breathing pulmonary ZTE is feasible and may serve as an alternative method in chest imaging. Either axial or sagittal ZTE image acquisition would be preferred in clinical practice.

1. Introduction

High-resolution computed tomography (HRCT) remains the first choice in the evaluation of lung diseases for its superb spatial resolution which is close to gross pathology [1]. However, the main concern about HRCT is the potentially harmful radiation despite low-dose approaches such as automatic tube current modulation, beam-sharpening filters, dynamic z-axis collimation, and iterative

* Corresponding author.
E-mail address: dengyu@gzhmu.edu.cn (Y. Deng).
[1] Qiuxi Lin and Cheng Cheng contributed equally to this work

https://doi.org/10.1016/j.heliyon.2024.e34098
Received 26 August 2023; Received in revised form 30 June 2024; Accepted 3 July 2024
Available online 4 July 2024

Abbreviations

ZTE	Zero echo time
NEX	Number of excitations
CT	Computed tomography
SNR	Signal-to-noise ratio
SI	Signal intensity
UTE	Ultra-short echo time
PETRA	Pointwise encoding time reduction with radial acquisition
TSE	Turbo spin-echo
IPAF	Interstitial pneumonia with autoimmune features
RA-ILD	Rheumatoid arthritis-associated interstitial lung disease

reconstruction algorithms [2]. Radiation exposure from CT scans in children, adolescents, and young adults is significantly correlated with an increased risk of hematologic malignancies [3]. Magnetic resonance imaging (MRI) is an attractive radiation-free tool in chest imaging, especially for children, pregnant women, and subjects who need to undergo repeated examinations for the purpose of tracking treatment response to lung cancer or diffuse lung diseases [4,5]. However, pulmonary MRI has been largely hampered by several conditions such as the overall low signal intensity of the low-proton-density lung tissues, the short-T2*-induced fast signal decay, and susceptibility artifacts at air-lung tissue interfaces [4]. In addition, the physiologic motion such as respiratory motion and cardiac pulsation may further degrade the image quality and devaluate image diagnostic efficacy. Cardiac pulsation and respiratory motion can be conquered by short acquisition time, multiple-breath-hold imaging, or respiratory triggering. However, many of the patients with respiratory diseases cannot tolerate long time or multiple breath-holding maneuvers due to shortness of breath.

Recently, pulmonary MR techniques either ultra-short echo time (UTE) or zero echo time (ZTE) have been applied to detect short T2* tissue such as cortical bone, fibrous cartilage, and pulmonary tissues [6,7]. In comparison with conventional MRI sequences, ZTE MRI sequence turns on readout gradient ahead of excitation with a high bandwidth and hard radiofrequency pulse, allowing gradient encoding to start instantaneously upon signal excitation, resulting in an actual TE of nominal zero. Therefore, it can detect short-T2 tissues. Moreover, the acoustical noise induced by gradient switching can be avoided in ZTE imaging [8]. Other advantages of ZTE MRI over conventional sequences in lung imaging include 1) 3D acquisition of high-resolution whole-lung images with multiplanar reconstruction (MPR) to display the morphological changes of the lung parenchyma; 2) A spiral acquisition for radial k-space fill-ins and respiratory gating enables free-breath scan and mitigates cardiac and respiratory motion artifacts; 3) Ahead-on gradual-increment readout gradient between successive repetitions achieves silent acquisition and provides a comfortable environment for patients [8]. However, most previous studies using ZTE have been focused on static organs such as the head and musculoskeletal systems [9], but few on lungs in human beings [10–12].

This study aimed to assess the feasibility of three-dimensional (3D) isotropic high-resolution lung MRI using a free-breathing zero-echo time imaging sequence on a 3.0 T MRI scanner. We compared the image quality and visibility of intrapulmonary structures in different acquisition planes and number of excitations (NEXs). Also, we tried to apply ZTE in a small sample of patients with interstitial lung diseases.

2. Materials and methods

2.1. Study population

The prospective study was approved by the Institutional Review Board of the first affiliated hospital of Guangzhou Medical University (No.2022–63; Date: 2022-06-26). The enrollment criteria for healthy volunteers were as follows: 1) Aged over 18; 2)No clear underlying lung diseases; 3) No respiratory-related symptoms such as cough, sputum, and dyspnea; 4) No claustrophobia. A total of thirty volunteers (16 males and 14 females) at a mean age of 26 years (aged 21–49 years) were enrolled in this study from October 2022 to May 2023. Furthermore, three patients (aged 39–56 years) with autoimmune-featured interstitial lung disease were included as well. Written informed consent was obtained from all subjects before the MRI scan.

2.2. MRI acquisition

All ZTE images were obtained using a 3.0 T MRI scanner (Discovery MR750w, GE Healthcare, Waukesha, WI) with a 32-channel body anterior phase-array coil and a 32-channel body array Geometry Embracing Method (GEM) coil. A commercially available respiratory belt (GE Healthcare) was wrapped around the patient's abdomen to capture the respiratory movement signal for triggering. All healthy subjects underwent free-breathing 3D isotropic lung ZTE image, image acquisition at the end of expiration, with a NEX of 2.5 in the supine position with overhead arms. Half of the subjects underwent both axial and coronal ZTE scans, and the other half underwent both axial and sagittal ZTE scans. Ten of the thirty subjects underwent an additional coronal ZTE scan with a NEX of 1.5. The imaging parameters of ZTE are shown in Table 1.

2.3. Image evaluation

Original coronal and sagittal images were reconstructed into axial images with slice thickness of 1.5 mm at GE AW4.7 post-processing workstation. All patient names, acquisition planes and NEX of all images were removed and randomized using random numbers by one radiologist (Dr. ZF Cai). Two radiologists (Dr. Y Deng and Dr. YY Bao, with 19 years and 6 years of experience in chest imaging, respectively) evaluated the images using the RadiAnt DICOM viewer (Version 2020.2.3, Medixant, Poland) independently and double-blinded to MR image parameters.

2.4. Overall image quality and visibility of intrapulmonary structures

Each reader rated the overall image quality of ZTE based on image artifacts, noise level, and signal uniformity using a four-point scale (1, poor; 2, fair; 3, good; 4, excellent). The standard reference images are shown in Fig. 1. The visibility of intrapulmonary structures including the bronchi, pulmonary arteries, and lung fissures were evaluated. The visible level of the bronchi (trachea deemed as the 1st generation, the main bronchi as the 2nd generation, the lobar bronchi as the 3rd generation, the segmental bronchi as the 4th generation, etc.) was rated. The visibility of pulmonary arteries was rated according to the following scale: 1, pulmonary trunk or the main pulmonary artery; 2, lobar pulmonary artery or the segmental pulmonary artery; 3, 5th, or 6th generation pulmonary artery; 4, 7th or 8th generation pulmonary artery; 5, more distal pulmonary artery. The visibility of the minor and major fissures was rated as invisible and visible. The aforementioned variables were documented as ordinal data.

2.5. Signal and signal-to-ratio of the lung parenchyma

The signal intensity (SI) and signal-to-noise ratio (SNR) of the lung parenchyma in the dependent (dorsal-peripheral) lung region and the non-dependent (anterior-peripheral and inner) lung region were measured by two readers (Fig. 2).

2.6. Clinical application in interstitial lung diseases

We present our preliminary experience in three young adults, including three patient (mean age, 46.7 ± 8.6 years) with interstitial lung disease. They were referred to our institution for routine follow-up, including CT. Patient 1 and patient 2 were female with interstitial pneumonia with autoimmune features (IPAF), age 39 and 56 years old, respectively. Patient 3 was a 45-year-old female with rheumatoid arthritis-associated interstitial lung disease (RA-ILD). Informed consent was obtained to perform additional lung MR imaging, within one week after a chest HRCT scan. ZTE protocol was consistent with the above axial NEX2.5 acquisition method. The imaging patterns were compared visually between ZTE and HRCT.

2.7. Statistical analysis

The continuous and category variables were described as mean ± standard deviation (SD) and percentiles, respectively. Cohen's kappa was used to evaluate the interobserver agreement for overall image quality, and the visibility of intrapulmonary structures (0–0.20, little agreement; 0.21–0.40, fair agreement; 0.41–0.60, moderate agreement; 0.61–0.80, substantial agreement; 0.81–1.00, almost perfect agreement between observers) [13]. The interobserver agreement of SI and SNR was calculated using the intraclass correlation coefficient (ICC) and Bland-Altman plots. An intraclass correlation coefficient greater than 0.70 is commonly considered a good agreement [14]. The normality of continuous variables was tested with the Shapiro-Wilk method. The overall image quality and the visibility of intrapulmonary structures between axial and coronal/sagittal scans were compared with the Wilcoxon signed-rank

Table 1
Parameters of 3D isotropic ZTE sequence.

	NEX 2.5			NEX 1.5
	Axial	Coronal	Sagittal	
TR (ms)	320	334	293	334
TE (ms)	0.02	0.02	0.02	0.02
Flip angle (°)	2	2	2	2
Acquisition plane	Axial	Coronal	Sagittal	Coronal
FOV (mm)	320–360	320–340	280–340	320–360
Pixel size (mm)	1.5 × 1.5	1.5 × 1.5	1.5 × 1.5	1.5 × 1.5
Spokes per segment	256	256	256	256
Slice thickness (mm)	1.5	1.5	1.5	1.5
Slice numbers	128–180	126–150	160–210	142–170
Bandwidth (kHz)	62.5	62.5	62.5	62.5
Reconstruction matrix	512 × 512	512 × 512	512 × 512	512 × 512
Intensity correction method	pure	pure	pure	pure
Mean TA (range) (s)	481.2 (379.2–554.4)	376.8 (308.4–445.2)	394.8 (314.4–549.6)	253.8 (188.4–390.0)

† Abbreviation: TR, repetition time; TE, echo time; TA, total acquisition time; FOV, field of view.

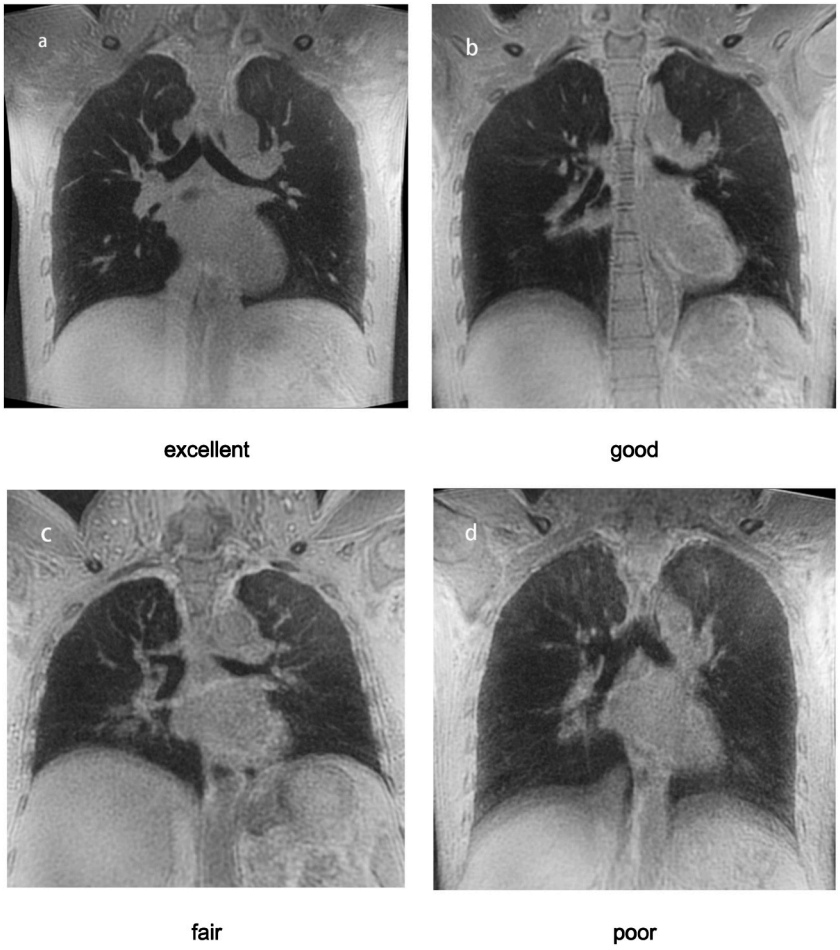

Fig. 1. The illustrated standard reference images were rated as excellent, good, fair and poor respectively for assessing the overall Image quality of ZTE images, based on image artifacts, noise level, and signal uniformity.

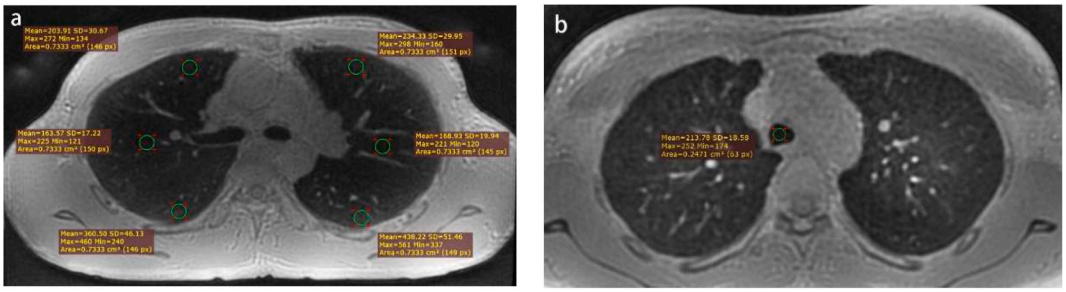

Fig. 2. An example of signal intensity and SNR measurements of lung parenchyma. (a) Six identical ROIs with about 150 pixels were placed in the anterior-peripheral, inner, and dorsal-peripheral lung region on both lungs at the trachea bifurcation section while avoiding bronchi and vessels. (b) The standard deviation (SD) of the SI measured in the tracheal lumen at the aortic arch section was considered as noise. SNR was calculated as the mean SI of the lung divided by noise.

test. The SI and SNR between different lung regions were also compared with the Wilcoxon signed-rank test. The image quality between Coronal NEX 2.5 and NEX 1.5 was compared with the Mann-Whitney *U* test. Statistical analyses were performed using MedCalc 19.5.6 (MedCalc Software Ltd, Belgium) or SPSS 22.0 (IBM, Chicago, IL). A *P*-value of <0.05 was considered statistically significant for all tests.

3. Results

3.1. Interobserver agreement

The Kappa value for interobserver agreement was 0.686 for the overall image quality, 0.744 for the visibility of bronchi, 0.666 for the visibility of pulmonary artery, 0.813 for the visibility of minor fissure, 0.697 for the visibility of major fissure, and 0.744 for the sum score of visibility of fissures. The ICC for SI and SNR was 0.898 (95 % CI, 0.802–0.949) and 0.806 (95 % CI, 0.639–0.900), respectively. Bland-Altman plots showed the interobserver agreements of SI and SNR (Fig. 3).

The overall image quality, visibility of bronchi, pulmonary artery, and fissures in axial scan with NEX 2.5.

The overall image quality was good to excellent for twenty-eight healthy subjects (93.3 %), and fair for two cases (6.7 %) due to severe respiratory motion artifact. Up to the fourth generation of the bronchi were visible in most subjects (25/30, 83.4 %), and the fifth generation was visible in one subject. The sixth or seventh generation of the pulmonary arteries was visible in 18 subjects (60 %) (Fig. 4). Minor and major fissures can be visualized in 23.3 % (7/30) and 56.7 % (17/30) of all subjects, respectively (Table 2). A lung nodule was incidentally found in two participants (Fig. 5). An azygos fissure was found in one participant (Fig. 6).

3.2. Comparison of the SI and SNR between different lung regions

The mean SI and SNR (407.4 ± 67.2 and 22.8 ± 7.1) of the dependent (dorsal-peripheral)lung region were higher than those (240.2 ± 44.6 and 13.5 ± 4.5, 210.0 ± 43.7 and 11.6 ± 3.4, respectively) of the non-dependent (anterior-peripheral, inner) lung region ($P < 0.001$). The mean SI and SNR (240.2 ± 44.6 and 13.5 ± 4.5, 407.4 ± 67.2 and 22.8 ± 7.1, respectively) of the peripheral (anterior-peripheral, and dorsal-peripheral) lung region were higher than those (210.0 ± 43.7 and 11.6 ± 3.4) of the inner region (*both* $P < 0.001$) (Fig. 7).

Comparison of image quality, the visibility of intrapulmonary structures between axial, coronal, and sagittal scans, as well as between coronal NEX 2.5 and NEX 1.5 scans.

The overall image quality, the visibility of the pulmonary artery, and fissures were better in the axial scan than in the coronal one ($P = 0.011$, 0.008, 0.010, respectively) but not of the bronchus ($P = 0.083$). There was no difference in the overall image quality, the visibility of bronchus, pulmonary artery, and fissures between axial and sagittal scan, as well as between coronal NEX 2.5 and NEX 1.5 (All $P > 0.05$) (Table 3).

3.3. Initial experience in interstitial lung diseases

Illustrated HRCT and ZTE images of three patients were shown in Fig. 8. The imaging patterns of ILD such as consolidation, reticular opacities, honeycombing, and ground-glass opacities demonstrated by ZTE were comparable to HRCT.

4. Discussion and conclusion

3D isotropic high-resolution lung ZTE MRI under free-breathing condition is friendly to patients with lung dysfunction and feasible to display a lot of intrapulmonary structures such as segmental bronchi, subsegmental, distal pulmonary arteries, and even fissures in a healthy cohort.

Free-breathing whole lung ZTE imaging with an isotropic resolution of 1.5 mm was successfully implemented in this study. The overall image quality of lung ZTE was good to excellent in most subjects (93.3 %). The most distal visible bronchi in this study were up to the fifth generation (subsegmental level) in 3.3 % of subjects. This finding was comparable to the study using a pointwise encoding time reduction with radial acquisition (PETRA) sequence, where the sixth bronchial generation (subsegmental level) bronchi remained

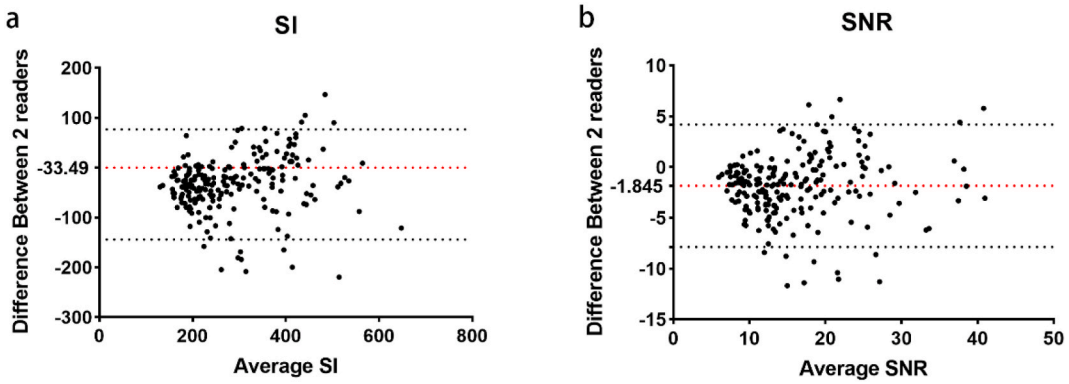

Fig. 3. Bland-Altman plots for the interobserver agreements of (a) signal intensity (SI) and (b) signal-to-noise ratio (SNR). † The red and black dotted line represents mean bias and 95 % Limits of Agreement.

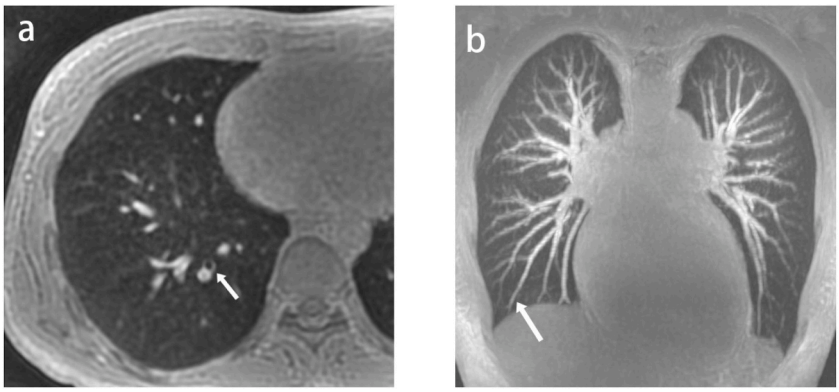

Fig. 4. Visibility of lung structures. (a) The posterior segmental bronchus (4th generation) of the right lower lobe (arrow) was well depicted by ZTE. (b) The 7th generation of the pulmonary artery in the right lower lobe (arrow) was well displayed using maximum intensity projection (MIP) for ZTE images. † MIP was not used for evaluating pulmonary artery visibility in this study, and this figure is shown only to facilitate distal pulmonary artery presentation.

Table 2
The evaluation of overall image quality, and the visibility of pulmonary bronchi, pulmonary arteries, and fissures.

The evaluation of image quality and visibility of intrapulmonary structures	
	Subjects (n = 30)
Overall Image Quality	
1, poor	0 (0 %)
2, fair	2 (6.7 %)
3, good	7 (23.3 %)
4, excellent	21 (70.0 %)
Visibility of the most distal bronchi	
3rd, lobar bronchus	4 (13.3 %)
4th, segmental bronchus	25 (83.4 %)
5th, subsegmental bronchus	1 (3.3 %)
Visibility of the most distal pulmonary arteries	
3rd (lobar) to 4th (segmental) generation of pulmonary artery	1 (3.3 %)
5th (subsegmental) to 6th generation of pulmonary artery	11 (36.7 %)
7th to 8th generation of pulmonary artery	18 (60.0 %)
Visibility of the fissures	
Major fissure	17 (56.7 %)
Minor fissure	7 (23.3 %)

† Numbers in parentheses are percentages.

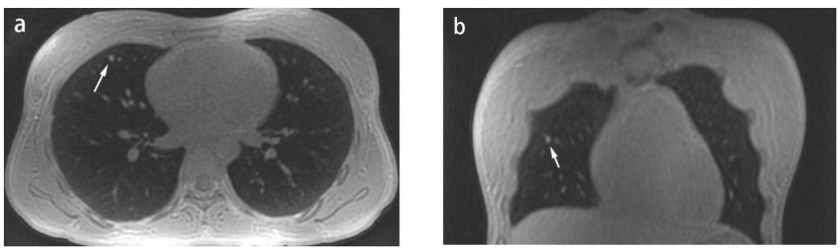

Fig. 5. An incidental lung nodule on ZTE images. Both (a) axial and (b) coronal image displayed a well-margined solid nodule in the right middle lobe which most likely represents an intrapulmonary lymph node (arrow).

visible in 2.2 % of cases (42/1920) [15]. The more distal pulmonary arteries (up to the 7th to 8th generation) were more visible than bronchi on ZTE images in 60 % of subjects, attributing to the intrinsic characteristics of the bronchus such as the thin wall, scarce proton in the lumen, and air-tissue interface induced magnetic susceptibility. Recently, a study compared the image quality between UTE and ZTE in healthy volunteers and showed the depiction of peripheral bronchi and small pulmonary arteries was superior in ZTE [10]. Lung fissures are a double-fold of visceral pleura that either completely or incompletely invaginate lung parenchyma to form the lung lobes. Each lung has an oblique fissure separating the upper lobes from the lower lobes, and the right lung has a horizontal fissure

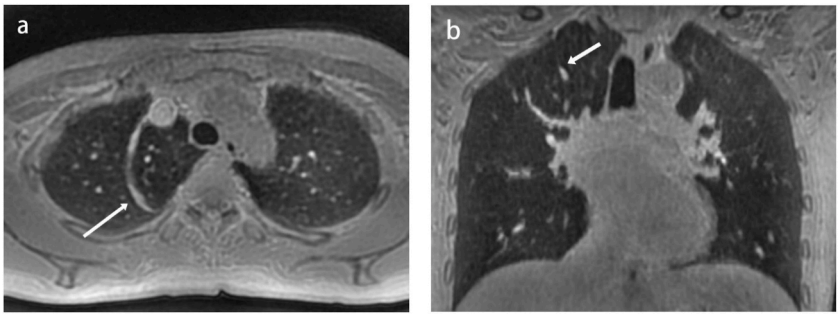

Fig. 6. The azygos fissure on ZTE images. Both (a) axial and (b) coronal image demonstrated the azygos fissure and vein (arrow).

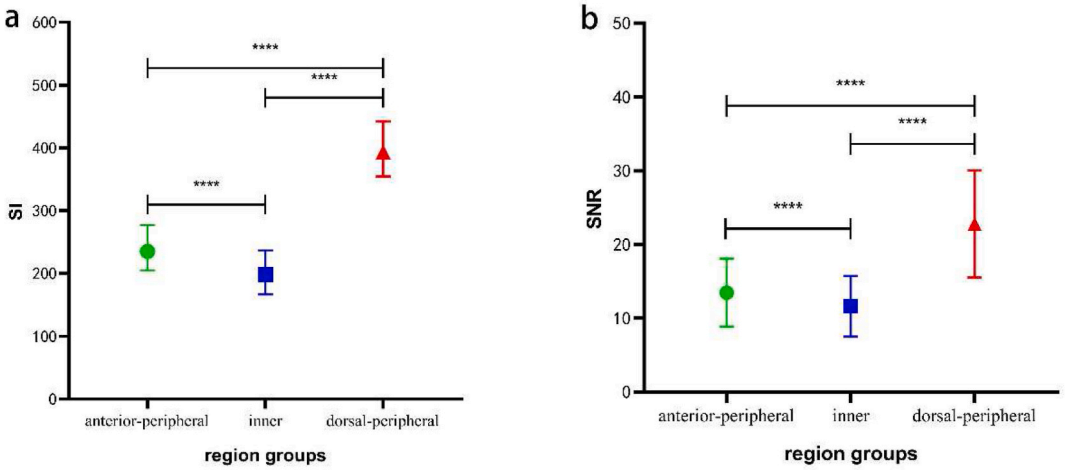

Fig. 7. Comparison of the mean (a) SI and (b) SNR between different lung regions. (a) The mean SI of the dependent lung region was higher than that of the non-dependent, and the mean SI of the peripheral lung was higher than that of the central lung; (b) The mean SNR of the dependent lung was higher than that of the non-dependent lung, and the mean SNR of the peripheral lung was higher than that of the central lung. † ****$P < 0.001$. Under the sample size of N = 73 in each group and the significance level of 0.05, all the statistical powers of pairwise comparisons between groups were greater than 0.99.

Table 3
Comparison of image quality, and the visibility of intrapulmonary structures between various acquisition planes and NEX.

		NEX 2.5		*P* value	NEX2.5		*P* value	Coronal		*P* value
		axial	coronal		axial	Sagittal		NEX2.5	NEX1.5	
Overall image quality		3.67 ± 0.62	3.13 ± 0.92	0.011*	3.60 ± 0.63	3.60 ± 0.83	1.000	3.13 ± 0.92	3.23 ± 0.60	1.000
The visibilities of intrapulmonary structures	Bronchus	3.87 ± 0.35	3.67 ± 0.49	0.083	3.93 ± 0.46	3.87 ± 0.64	0.564	3.67 ± 0.49	3.92 ± 0.28	0.254
	Pulmonary arteries	3.67 ± 0.49	3.20 ± 0.56	0.008*	3.47 ± 0.64	3.40 ± 0.63	0.564	3.20 ± 0.56	3.31 ± 0.48	0.717
	Fissures	0.80 ± 0.68	0.20 ± 0.41	0.010*	0.80 ± 0.86	1.13 ± 0.83	0.059	0.20 ± 0.41	0.31 ± 0.48	0.650

† Data are means ± standard deviations. *$P < 0.05$. In NEX 2.5 - axial vs. coronal comparison, the results of overall image quality and visibility of pulmonary arteries which were considered as statistically significant, were with the statistical powers of 0.85 and 0.90 respectively under the sample size of N = 15 in each group and the significance level of 0.05.

that separates the right upper lobe from the middle lobe. In this study, the minor and major fissures were partially visualized in 23.3 % (7/30) and 56.7 % (17/30) of all subjects, respectively. The major fissures were more visible than the minor fissure due to its greater length and thickness. Our results were inconsistent with the previous PETRA study in which the visibility of fissures was graded as higher as 3.8 ± 0.4 (a grade of 4 deemed as good complete visibility) [15]. It may be attributed to the fact that the voxel size in the previous study was smaller than current study (0.86 mm^3 vs. 1.5 mm^3). However, lung fissures are often incomplete even absent and the prevalence of complete fissures is around 50–70 % in adults, which further increases the difficulty in the depiction by MRI [16,17].

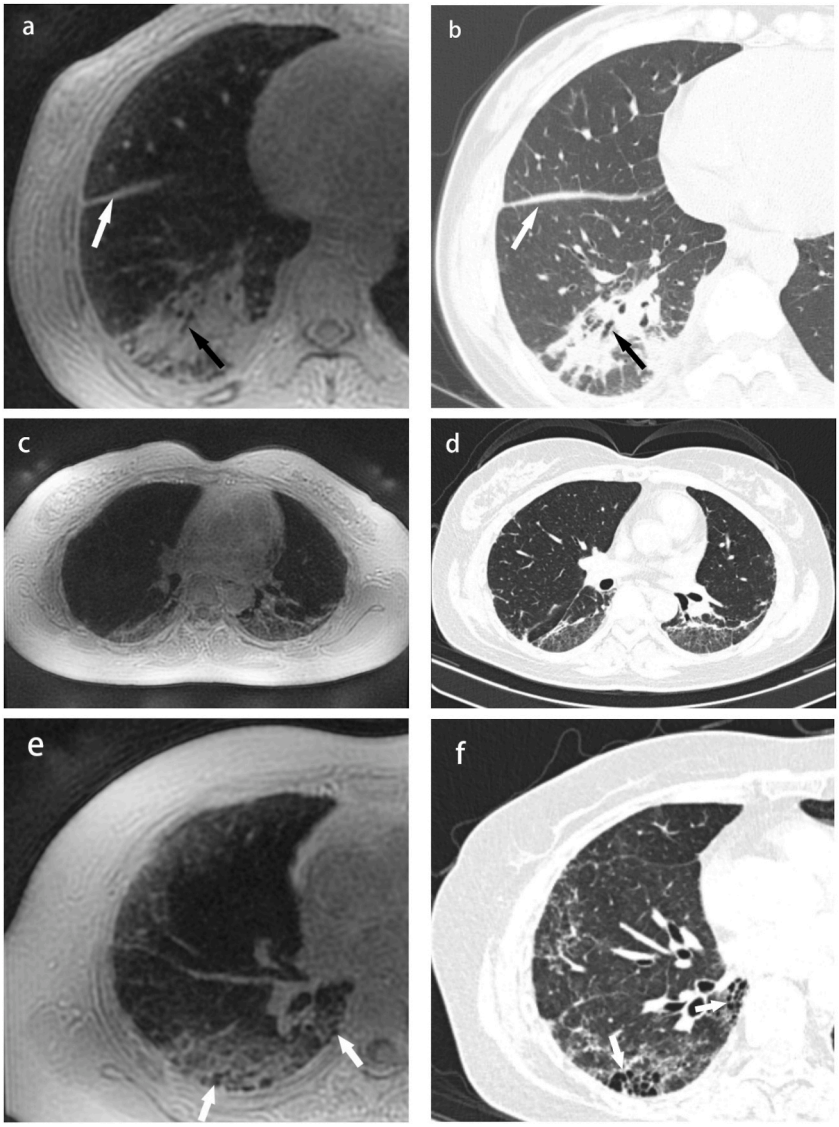

Fig. 8. (a) Axial ZTE and (b) CT images of the lung acquired in a 39-year-old female with IPAF. Patchy high-signal replacing normal alveolar signal in the posterior basal segment of the right lower lung at ZTE image, concordant with consolidation at CT image. Besides, air bronchogram (black arrows) and effusion of pulmonary fissure (white arrows) can be demonstrated in both techniques. (c) ZTE and (d) CT images acquired in a 45-year-old female with RA-ILD. Reticular and ground-glass opacities, located at the dorsal subpleural of both lower lungs, can be detected on ZTE imaging similar to the HRCT. (e) Axial ZTE and (f) CT images of the lung acquired in a 56-year-old female also with IPAF. ZTE shows a cluster of honeycombing (white arrows) located at the dorsal subpleural of the right lower lung, in agreement with HRCT. † ZTE and HRCT images were acquired at the end of the expiratory phase and the inspiratory phase respectively, resulting in a discrepancy in the location of the lesions between the two modalities.

Accessory fissures of the lung are the most common variants in pulmonary development, including azygos fissure, inferior accessory fissure, superior accessory fissure, and left horizontal fissure [18]. An azygos fissure in one subject was incidentally found in this study, which indicates ZTE would be good at displaying lung anatomy and congenital anomalies.

Our study demonstrated the signal intensity and SNR varied across different lung regions. First, the signal intensity and SNR of the dependent lung region were higher than that of the non-dependent lung region, which is visually appreciated as vertical increased signal intensity along the direction of gravity. This result was consistent with previous studies that the lung was imaged with contrast-enhanced perfusion [19] and multiple inversion turbo spin-echo (TSE) sequences [20]. Recently, these phenomena were also found in both ZTE and UTE in a healthy children lung MRI cohort [21]. This observation could be exquisitely explained by the inhomogeneous distribution of regional lung density and perfusion [20,22]. Interestingly, our study also found that the signal intensity and SNR of the anterior-peripheral lung region were higher than that of the central region. We propose this difference might contribute to the inherently inhomogeneous reception profile of the surface coil detector, in which the signal among different lung regions relies on the

distance to the phased-array coils. Besides, the motion related to cardiac pulsation could be a reason as well, which may accelerate T2* signal decay of the inner zone lung parenchymal. As a result, mild abnormalities in the central lung parenchyma may be hardly demonstrated because of the overall low signal intensity of the region. Several signal correction methods including discrete-time wavelet transform and wavelet packet have been studied and approached in the brain or spine [23,24]. However, more sophisticated and robust postprocessing techniques or algorithms dedicated to the lung remain a challenge due to the much lower proton density of the lung than other organs.

Few studies have explored the feasibility of ZTE for lung parenchymal imaging, especially several influential factors such as NEX and imaging plane might on image quality [10,12]. To better clinically apply high-resolution ZTE lung imaging, we firstly explore better ZTE MR imaging parameters via comparison of the image quality and visibility of lung structures among different acquisition planes of ZTE MR imaging in humans. Interestingly, the axial scan showed better overall image quality and visibility of intrapulmonary structure than the coronal scan while no different from the sagittal scans. This observation might be due to the larger FOV used in axial and sagittal scan than in coronal scan, which leads to higher SNR. As a result, ZTE with either axial or sagittal scan would be preferred in clinical practice.

Most previous studies have adopted NEX 1.5 or 1.0 for lung imaging either by UTE or ZTE [10,11,15]. Higher NEX increases SNR while multiple signal excitations are also effective for reducing motion and pulsation artifacts. For this purpose, we compared the image quality between NEX 2.5 and NEX 1.5. In this small-sample study, the increase in NEX did not appear to provide additional benefits in terms of overall image quality and visibility of intrapulmonary structures but extended acquisition time. This may be subject to current resolution. If the patient cannot tolerate a long scan time, NEX 1.5 would be an alternative option with enough diagnostic image quality.

This study had several limitations. Firstly, this study investigated the quality of pulmonary ZTE during free breathing, respiration rate could have had an impact on the image quality. Limited by sample size, it is not very convincing to analyze the impact of the respiratory rate on the image quality. Secondly, only a few patients with ILDs were included in this exploratory study. Considering that most subjects were healthy volunteers, it remains uncertain whether this sequence can be widely applied to patients with pulmonary pathologies. Further studies with larger populations are required to confirm our preliminary results.

In conclusion, 3D isotropic high-resolution lung ZTE MRI under free-breathing condition is feasible and promises to serve as an alternative option for chest imaging with diagnostic image quality and spatial resolution. ZTE image acquisition with either axial or sagittal scan would be preferred in clinical practice. Further technical developments regard to the spatial resolution and acquisition time, as well as algorithms that deal with signal inhomogeneity may enhance the utility of ZTE for routine clinical lung imaging.

5. Data availability statement

Data will be made available on request.

Ethics declarations

All participants/patients provided informed consent to participate in the study.

Funding

This study was funded by National key R&D program of China (No. 2021YFC2500700) and Guangzhou Science and Technology Project (No. 2023A03J0359).

CRediT authorship contribution statement

Qiuxi Lin: Writing – original draft, Project administration, Formal analysis, Data curation, Conceptualization. **Cheng Cheng:** Formal analysis, Data curation. **Yingying Bao:** Formal analysis. **Weiyin Vivian Liu:** Writing – review & editing, Methodology. **Lei Zhang:** Software, Methodology. **Zhaofeng Cai:** Investigation. **Qi Wan:** Investigation. **Chongpeng Sun:** Investigation. **Xinchun Li:** Investigation. **Yu Deng:** Writing – review & editing, Resources, Project administration, Formal analysis, Conceptualization.

Declaration of competing interest

The authors declare that they have no known competing financial interests or personal relationships that could have appeared to influence the work reported in this paper.

Acknowledgements

We wish to thank Jianxun He, Donghe Han, Jiaxi Yu for technical guidance during the MRI scan, and Prof. Hongkai Wu for his help in statistics.

References

[1] M.B. Gotway, et al., High-resolution CT of the lung: patterns of disease and differential diagnoses, Radiol. Clin. 43 (3) (2005) 513, 42, viii.
[2] J.F. Gruden, et al., An algorithmic approach to the interpretation of diffuse lung disease on chest CT imaging: a theory of almost everything, Chest 157 (3) (2020) 612–635.
[3] M. Bosch de Basea Gomez, et al., Risk of hematological malignancies from CT radiation exposure in children, adolescents and young adults, Nat Med 29 (12) (2023) 3111–3119.
[4] J. Biederer, et al., MRI of the lung (3/3)—current applications and future perspectives, Insights Imaging 3 (4) (2012) 373–386.
[5] K.S. Sodhi, et al., Diagnostic utility of 3T lung MRI in children with interstitial lung disease: a prospective pilot study, Acad. Radiol. 25 (3) (2018) 380–386.
[6] H. Hatabu, et al., Expanding applications of pulmonary MRI in the clinical evaluation of lung disorders: fleischner society position paper, Radiology 297 (2) (2020) 286–301.
[7] Y. Tanaka, et al., State-of-the-art MR imaging for thoracic diseases, Magn Reson Med Sci. 21 (1) (2022) 212–234.
[8] M. Weiger, K.P. Pruessmann, F. Hennel, MRI with zero echo time: hard versus sweep pulse excitation, Magn. Reson. Med. 66 (2) (2011) 379–389.
[9] M. Weiger, et al., ZTE imaging in humans, Magn. Reson. Med. 70 (2) (2013) 328–332.
[10] K. Bae, et al., Comparison of lung imaging using three-dimensional ultrashort echo time and zero echo time sequences: preliminary study, Eur. Radiol. 29 (5) (2019) 2253–2262.
[11] K. Bae, et al., Respiratory motion-resolved four-dimensional zero echo time (4D ZTE) lung MRI using retrospective soft gating: feasibility and image quality compared with 3D ZTE, Eur. Radiol. 30 (9) (2020) 5130–5138.
[12] F. Gibiino, et al., Free-breathing, zero-TE MR lung imaging, Magma 28 (3) (2015) 207–215.
[13] H.L. Kundel, M. Polansky, Measurement of observer agreement, Radiology 228 (2) (2003) 303–308.
[14] A. Anvari, E.F. Halpern, A.E. Samir, Statistics 101 for radiologists, Radiographics 35 (6) (2015) 1789–1801.
[15] G. Dournes, et al., Quiet submillimeter MR imaging of the lung is feasible with a PETRA sequence at 1.5 T, Radiology 276 (1) (2015) 258–265.
[16] K. Hayashi, et al., Radiographic and CT appearances of the major fissures, Radiographics 21 (4) (2001) 861–874.
[17] S. Kc, et al., Variations in human pulmonary fissures and lobes: a study conducted in nepalese cadavers, Anat Cell Biol 51 (2) (2018) 85–92.
[18] J.D. Godwin, R.D. Tarver, Accessory fissures of the lung, AJR Am. J. Roentgenol. 144 (1) (1985) 39–47.
[19] K.W. Stock, et al., Demonstration of gravity-dependent lung perfusion with contrast-enhanced magnetic resonance imaging, J Magn Reson Imaging 9 (4) (1999) 557–561.
[20] A.A. Bankier, et al., Gravity-dependent signal gradients on MR images of the lung in supine and prone positions: a comparison with isogravitational signal variability, J Magn Reson Imaging 23 (2) (2006) 115–122.
[21] K.G. Zeimpekis, C.J. Kellenberger, J. Geiger, Assessment of lung density in pediatric patients using three-dimensional ultrashort echo-time and four-dimensional zero echo-time sequences, Jpn. J. Radiol. 40 (7) (2022) 722–729.
[22] H.M. Almquist, et al., Pulmonary perfusion and density gradients in healthy volunteers, J. Nucl. Med. 38 (6) (1997) 962–966.
[23] F.H. Lin, et al., A wavelet-based approximation of surface coil sensitivity profiles for correction of image intensity inhomogeneity and parallel imaging reconstruction, Hum. Brain Mapp. 19 (2) (2003) 96–111.
[24] H. Ren, W. Lin, X. Ding, Surface coil intensity correction in magnetic resonance imaging in spinal metastases, Open Med. 12 (2017) 138–143.